Results in Surfaces and Interfaces 12 (2023) 100131

Contents lists available at ScienceDirect

Results in Surfaces and Interfaces

journal homepage: www.elsevier.com/locate/rsurfi

# Influence of thermal and acidic treatments on the morphology of a natural kaolinitic clay mineral

Pierre Ngue Song [a], Julien G. Mahy [a,b,*], Cédric Calberg [a], Antoine Farcy [a], Joachim Caucheteux [a], Nathalie Fagel [c], Stéphanie D. Lambert [a]

[a] Department of Chemical Engineering – Nanomaterials, Catalysis & Electrochemistry, University of Liège, B6a, Quartier Agora, Allée du Six Août 11, 4000 Liège, Belgium

[b] Institut National de la Recherche Scientifique (INRS), Centre Eau Terre Environnement, Université du Québec, 490, Rue de la Couronne, Québec (QC), G1K 9A9, Canada

[c] Laboratoire Argiles, Géochimie et Environnements sédimentaires (AGEs), Department of Geology, Faculty of Sciences, University of Liège, Liège, B-4000, Belgium

ARTICLE INFO

*Keywords:*
Morphology modification
Porous clay
Adsorbent
Natural material valorization
Calcination

ABSTRACT

In this work, a natural kaolinitic clay mineral from Kribi in Cameroon is modified by thermal and acidic treatments. The influence of these treatments on the physicochemical properties of the clays is studied using X-ray diffraction, Fourier transform infrared spectroscopy, nitrogen adsorption–desorption measurements, scanning electron microscopy, inductively coupled plasma–atomic emission spectroscopy and thermal analysis. Three calcination temperatures are explored: 600, 700 and 800 °C. The XRD pattern of the untreated clay showed that the natural clay mineral was mostly composed of kaolinite. Calcination at high temperatures allowed the amorphization of the natural kaolinitic clay mineral to obtain metakaolinite. This heat treatment of the natural clay mineral produced disintegration by rupture of the strong hydrogen bonds between the layers of the clay mineral. Heat treatment did not increase the specific surface area of the clay, which stayed around 20-30 $m^2/g$. The acid treatment produced a high material texture modification giving microporous materials with a large surface area up to 315 $m^2/g$ with the sample previously calcined at 800 °C. The microporosity and mesoporosity increase is greater when the clay is calcined at high temperature. The morphology of the samples observed by SEM are modified by the acidic treatment. The initial two-dimensional stacking of particles evolves towards a narrower three-dimensional porous structure. These treatments open the way to produce highly porous clay materials that could be used as adsorbent materials for pollutant removal from water.

## 1. Introduction

Clay minerals are natural nanomaterials with various microstructures (Dong and Zhang, 2018; Zhou et al., 2016), such as nano-platelets and nanofibers. They also have many advantages such as being abundant in nature, inexpensive and environmentally friendly (Dong and Zhang, 2018; Zhou et al., 2016; Misra et al., 2018).

Kaolinite is an abundant clay mineral in nature (Gao et al., 2016). It is a 1:1 type aluminosilicate; that is, having tetrahedral sheets of silicate units ($SiO_4$) covalently bonded to octahedral sheets of hydroxylated ($AlO_6$) entities [$AlO_{(6-x)}$ $(OH)_x$] (as represented in Fig. 1), with the general composition $Al_2Si_2O_5(OH)_4$ (Hai et al., 2015; Liu et al., 2017; Panda et al., 2010; Torres-Luna and Carriazo, 2019).

The presence of hydrogen bonds between neighboring or adjacent kaolinite layers (He et al., 2013; Tang et al., 2017; Tao et al., 2014) holds them strongly together (Tao et al., 2014), and makes it difficult to modify this mineral in terms of exfoliation or delamination (Torres-Luna and Carriazo, 2019). In addition, this property prevents the free expansion of the interlayer space as in swelling clay minerals 2:1 (Bergaya and Lagaly, 2006).

Natural or modified kaolinite has important properties for various applications, such as the adsorption of organic and inorganic pollutants (Tang et al., 2017; Tao et al., 2014; Bergaya and Lagaly, 2006; Awwad et al., 2022; Aragaw and Alene, 2022; David et al., 2020; Jawad et al., 2022; Selvan et al., 2022), in the manufacture of reusable nanocomposites for photocatalytic disinfection (Misra et al., 2018; Gao et al., 2016; Hai et al., 2015; Liu et al., 2017; Panda et al., 2010; Torres-Luna and Carriazo, 2019; He et al., 2013; Tang et al., 2017; Tao et al., 2014; Bergaya and Lagaly, 2006; Awwad et al., 2022; Aragaw and Alene, 2022; David et al., 2020; Jawad et al., 2022; Selvan et al., 2022; Misra et al., 2022; Zhao et al., 2021) and finally in the preparation of superhydrophobic coatings (Dong and Zhang, 2018; Zhou et al., 2016;

* Corresponding author at: Department of Chemical Engineering – Nanomaterials, Catalysis & Electrochemistry, University of Liège, B6a, Quartier Agora, Allée du Six Août 11, 4000 Liège, Belgium.
*E-mail address:* julien.mahy@uliege.be (J.G. Mahy).

https://doi.org/10.1016/j.rsurfi.2023.100131
Received 28 April 2023; Received in revised form 6 July 2023; Accepted 12 July 2023

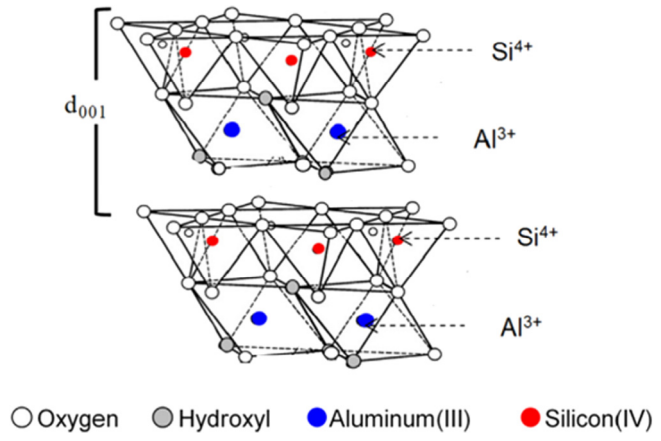


**Fig. 1.** General structure of kaolinite, reproduced from.

Misra et al., 2018; Gao et al., 2016; Hai et al., 2015; Liu et al., 2017; Panda et al., 2010; Torres-Luna and Carriazo, 2019; He et al., 2013; Tang et al., 2017; Tao et al., 2014; Bergaya and Lagaly, 2006; Awwad et al., 2022; Aragaw and Alene, 2022; David et al., 2020; Jawad et al., 2022; Selvan et al., 2022; Misra et al., 2022; Zhao et al., 2021; Qu et al., 2017).

In the last decade, the development of different surface treatment techniques for improving the reactivity of kaolinite has experienced a significant increase. These include heat treatments and the graft bypass (Ebrahimi et al., 2020; Elimbi et al., 2011; Kenne Diffo et al., 2015; Nmiri, 2017; Reli et al., 2014; Soleimani et al., 2012) that improves the reactivity of kaolinite by chemically modifying it. This can be achieved either by the immobilization of an active species on the surface of the kaolinite (Hai et al., 2015) or by the intercalation of organic molecules in kaolinite's interfoliar space (He et al., 2013; Tang et al., 2017; Tao et al., 2014; Bergaya and Lagaly, 2006; Awwad et al., 2022; Aragaw and Alene, 2022; David et al., 2020; Jawad et al., 2022; Selvan et al., 2022; Misra et al., 2022; Zhao et al., 2021; Qu et al., 2017; Ebrahimi et al., 2020; Elimbi et al., 2011; Kenne Diffo et al., 2015; Nmiri, 2017; Reli et al., 2014; Soleimani et al., 2012; Abbassi et al., 2021; Guerra et al., 2012).

Another more effective approach to activate kaolinite is acid treatment that can significantly increase the specific surface area (Ji and Zhang, 2021; Paredes-Quevedo et al., 2021). The $Al^{3+}$ cations of the octahedral sheet are more reactive to acid than the $Si^{4+}$ of the tetrahedral sheet (Hai et al., 2015; Liu et al., 2017; Panda et al., 2010; Torres-Luna and Carriazo, 2019; He et al., 2013; Tang et al., 2017; Tao et al., 2014; Bergaya and Lagaly, 2006; Awwad et al., 2022; Aragaw and Alene, 2022; David et al., 2020; Jawad et al., 2022; Selvan et al., 2022; Misra et al., 2022; Zhao et al., 2021; Qu et al., 2017; Ebrahimi et al., 2020; Elimbi et al., 2011; Kenne Diffo et al., 2015; Nmiri, 2017; Reli et al., 2014; Soleimani et al., 2012; Abbassi et al., 2021; Guerra et al., 2012; Ji and Zhang, 2021; Paredes-Quevedo et al., 2021; Lenarda et al., 2007). This leads to the elimination of $Al_2O_3$ and the formation of a porous solid, composed mainly of amorphous $SiO_2$ (Belver et al., 2002). These treatments can enhance the adsorption properties of a natural clay for use in depollution applications.

The goal of this work is to study the influence and contribution of heat treatment in a highly concentrated hydrochloric acid medium under reflux conditions on a kaolinitic clay from Kribi (region of southern Cameroon) in the development of microporosity and mesoporosity, and the specific surface area. The optimized conditions of treatment to obtain the best adsorbent material from natural clay will be determined. Three temperatures will be explored: 600, 700 and 800 °C. The acidic treatment will be applied before or after calcination. The objective is to produce a highly porous material from natural clays that are abundantly present in Africa and could be used as low cost, efficient adsorption materials for organic pollutant removal in water. To explore their physicochemical properties as modified by the heat and acidic treatments, X-ray diffraction, nitrogen adsorption–desorption measurements, scanning electron microscopy, inductively coupled plasma–atomic emission spectroscopy and thermal assays will be performed. Finally, the materials will be tested as adsorbents for malachite green removal from water.

## 2. Experiments

### 2.1. Clay material

The kaolinitic clay mineral used in this work comes from the Kribi deposit in the southern region of Cameroon. Demineralized water was used to wash the clay mineral as well as during its purification by extraction of the ≤ 2 μm fraction. Two dispersing agents from Sigma-Aldrich, i.e., sodium hexametaphosphate ($Na_6(PO_3)_6$) and hydrochloric acid (HCl, 37%), were used for chemical activation.

### 2.2. Clay washing and purification

The clay mineral-rich materials underwent two successive wet washes with demineralized water: the first using an 80 μm sieve; the second using a 50 μm sieve. Purification was achieved by extraction of the clay fraction ≤ 2 μm by sedimentometry using a particle size analyzer (Micrometrics SediGraph@III Plus (AGEs, ULiège)). This form of purification is based on the difference in density of the mineral species that make up the clay material. Quartz is one of the major impurities in our material, with contents above 12%. The literature suggests that the equivalent diameters are generally less than 2 μm, Elimbi et al. (2011). It is therefore possible, taking into account this property and the densities of quartz and clay mineral species, to enrich the material in clay mineral species using the sedimentometry process (Elimbi et al., 2011).

The principle of sedimentometry and therefore the extraction of the clay fraction from a suspension in water is based on Stoke's law (Yans and Lithostratigraphie, 2007). In general, for a spherical particle, we have the relation:

$$t = \frac{190x}{D^2} \quad (1)$$

Where $t$ is the sedimentation time (min); $D$ is the particle diameter (μm); $x$ is the depth of descent (in cm) of the particles of diameter $D$.

Sedimentation is carried out at 25 °C in a 20 L capacity cylindrical container with two taps located vertically 24 cm apart. The material resulting from the preliminary treatment is soaked in demineralized water containing sodium hexametaphosphate ($Na_6(PO_3)_6$) (dispersing agent). The container contents are homogenized by mechanical agitation and left to stand for 45 to 50 minutes (sedimentation time). The clay suspension is collected by opening the first tap located at the top at a depth of 27 cm. The rest of the container is once again homogenized by mechanical agitation and the < 2 μm clay fraction is collected by opening the second, lower tap located at a depth of 8 cm. The collected clay solution is left to settle under atmospheric air for 3 days. After removing the supernatant, the clay paste obtained is dried in an oven at 105 °C until a constant weight is reached. The obtained dried extracts are then ground and sieved at 80 μm. This material is herein called KAO.

### 2.3. Thermal treatments

Twenty-three g of the ≤ 2 μm fraction (later defined as *clay*) is placed in a ceramic crucible, the clay is calcined at three temperatures (600, 700 and 800 °C) under air atmosphere, in a chamber furnace. The heating rate used is 10 °C/min from ambient temperature to the calcination temperature (600, 700 or 800 °C). Once the temperature level (600, 700 or 800 °C) is reached, it is maintained for 10 h. Then the temperature is decreased to 40 °C before removing the material. The mass losses recorded are around 12 to 13% of the initial mass of kaolinite. The obtained metakaolinites are named MK-T, $T$ being the calcination temperature.

### 2.4. Chemical activation with acid

Six g of the ≤ 2 μm clay fraction or one of the 3 materials obtained after calcination is mixed with 180 mL of a 6 M HCl solution in a three-necked flask topped with a reflux column. This mixture is then slowly heated to 110 °C with constant stirring under reflux conditions for 5 h. After cooling to room temperature, the acid-treated powder is separated from the solution by centrifugation at 15500 rpm using a SIGMA 3-30KS centrifuge with a 12159-H rotor equipped with six tubes. The residue obtained is washed with demineralized water until the filtrate has a neutral pH, then dried in an oven at 60 °C. The different powders obtained after the acid treatment are designated KAO-HCl, or MK-T-HCl, with $T$ being the calcination temperature.

### 2.5. Material characterization assays

The actual composition of the clays is determined by inductively coupled plasma–atomic emission spectroscopy (ICP–AES), using an ICAP 6500 Thermo Scientific device. The mineralization is fully described in Mahy et al. (2016) except that HF is used instead of $HNO_3$.

The crystallographic properties are observed through the X-ray diffraction (XRD) patterns recorded with a Bruker D8 Twin-Twin powder diffractometer using Cu-$K_\alpha$ radiation, with a step size of 0.002° and scan speed of 2°/min.

The specific surface area of samples is determined by nitrogen adsorption–desorption isotherms in an ASAP 2420 multi-sampler volumetric device from Micromeritics at −196 °C.

Scanning electron microscope (SEM) micrographs are obtained using a TESCAN Clara microscope under high vacuum at an acceleration voltage of 15 keV.

Fourier transform infrared (FT-IR) spectra in the region of 400–4000 $cm^{-1}$ are recorded at room temperature with a Thermo Nicolet Nexus FTIR spectrometer (Laboratoire de Minéralogie, ULiège). All catalyst powders are dispersed in KBr (1 wt % for all samples)

Thermogravimetric analysis (TGA) and differential scanning calorimetry (DSC) is carried out with a Simultaneous Thermal Analyzer Mettler-Toledo TG-DSC3$^+$ (AGEs, ULiège), under a nitrogen atmosphere. Ten mg of sample are placed in an alumina crucible and heated from 30 to 1100 °C with a heating rate of 10 °C/min.

### 2.6. Preliminary adsorption experiments

The adsorption tests are evaluated on the 8 clay samples at a constant pH of 7.3 at 25 °C. The model pollutant used for adsorption experiments is malachite green oxalate salt (MG, Sigma-Aldrich); 100 mg of clay sample is mixed with 20 mL of pollutant solution in water. The different samples are shaken continuously in the dark. Aliquots of pollutants are taken every 10 min up to 80 min. Concentrations are assessed with a Genesis 10S UV–Vis spectrophotometer (Thermo Scientific), a calibration curve was made previously to assess linearity with the concentration. The initial MG solution concentration is 100 mg/L. The main adsorption peak is located at 617 nm for malachite green.

## 3. Results and discussion

### 3.1. Crystalline composition

Fig. 2a shows the X-ray diffractograms for all the samples and Fig. 2b shows the peak attribution (on KAO sample). Fig. 2b reveals that kaolinite is the main mineral in this clay fraction, characterized by a reflection peak at $2\Theta = 12.4°$. The observed reflection centered at 24.9° is the secondary diffraction of the plane (0 0 1). Since the $02l$ *and* $11l$ sequences (20–23° 2q using $CuK\alpha$) are very sensitive to structural defects of the kaolinite (Fig. 3), the empirical relationship based on the weighted peak intensity ratio can be used to assess the degree of disorder of the kaolinite (Chmielová and Weiss, 2002). The determined values of the Hinckley index (HI), the Aparicio-Galán-Ferrell index (AGFI) and the weighted intensity ratio index (WIRI) are 1.039, 0.82 and 0.58 respectively. These values are close to those obtained by Ptáček et al. (2010); they correspond to the average degree of structural order of the applied kaolin (Chmielová and Weiss, 2002). However, the XRD diagrams (Fig. 2a) of kaolinite calcined at 600, 700 and 800 °C indicate the presence of a diffraction halo peak at $2\Theta$ between 18 and 30° characteristic of the amorphous phase present in metakaolinites (Elimbi et al., 2011; Kenne Diffo et al., 2015; Nmiri, 2017; Reli et al., 2014; Soleimani et al., 2012; Abbassi et al., 2021; Guerra et al., 2012; Ji and Zhang, 2021; Paredes-Quevedo et al., 2021; Lenarda et al., 2007; Belver et al., 2002; Yans and Lithostratigraphie, 2007; Mahy et al., 2016; Chmielová and Weiss, 2002; Ptáček et al., 2010; Bich et al., 2009; Panias et al., 2007). The peaks of kaolinite disappeared, as did the reflections of illite and those of gibbsite present as impurities. Similarly, the XRD pattern (Fig. 2a) of kaolinite having directly undergone the acid treatment (KAO-HCl) did not show significant variations under these experimental conditions compared to that of natural kaolinite (KAO). Only the disappearance of the reflection peaks of the gibbsite present as an impurity was recorded. This is accompanied by a slight increase in the intensity of quartz reflection due to the disappearance of the other crystalline phases with the treatments as also observed by Zhou et al. (2021). Based on the authors' previous works, hot acid treatment accelerates the interface reactions of clay minerals (Zhou et al., 2021; Jia et al., 2019). This characteristic of kaolinite being resistant to acid leaching has also been reported by other authors (Torres-Luna and Carriazo, 2019; He et al., 2013; Tang et al., 2017; Tao et al., 2014; Bergaya and Lagaly, 2006; Awwad et al., 2022; Aragaw and Alene, 2022; David et al., 2020; Jawad et al., 2022; Selvan et al., 2022; Misra et al., 2022; Zhao et al., 2021; Qu et al., 2017; Ebrahimi et al., 2020; Elimbi et al., 2011; Kenne Diffo et al., 2015; Nmiri, 2017; Reli et al., 2014; Soleimani et al., 2012; Abbassi et al., 2021; Guerra et al., 2012; Ji and Zhang, 2021; Paredes-Quevedo et al., 2021; Lenarda et al., 2007). Fig. 2a shows the XRD patterns of kaolinite calcined at 600, 700 and 800 °C and having undergone the hot acid treatment under reflux conditions. Compared to the metakaolinite samples, these patterns show a significant increase in the intensity of the reflection peak with a wide band between 20 and 30 °2q. The intensity of the reflection peak and the band width increase with the calcined temperature. These modifications observed on the XRD patterns are due to a significant increase in the quantity of amorphous silica generated by the acid treatment of the metakaolinites under reflux conditions, in agreement with Lenarda et al. (2007), Belver et al. (2002). The difference in reactivity to acid treatment between kaolinite and metakaolinite is explained by the fact that dehydroxylation occurs when kaolinite is calcined above 450–500 °C producing metakaolinite. This transformation involves the loss of structural water accompanied by a reorganization of the structure. Only part of the $AlO_6$ octahedra is preserved, while the major part is transformed into more reactive tetra and penta coordinate units (Lambert et al., 1989).

### 3.2. Chemical composition

Table 1 presents the results of the elemental analyses by ICP-AES, which made it possible to determine the chemical composition, as well as the concentration in mg/kg of dry matter of the major and minor elements present in the natural kaolinitic clay and some modified samples (KAO-HCl, MK-800 and MK-800-HCl). The clay mineral (KAO) used in this work is an aluminosilicate, given the high concentrations in mg/kg of dry matter of aluminum (168 000) and silicon (130 000). The concentration in mg/kg of iron dry matter is 6290 and that of titanium 10 700, corresponding to an aluminosilicate mineral with low $Fe_2O_3$ and $TiO_2$ contents.

However, chemical analysis also provides evidence that kaolinite is resistant to acid leaching because hot acid treatment only reduced the concentration of aluminum solids by 30%. In contrast, that of

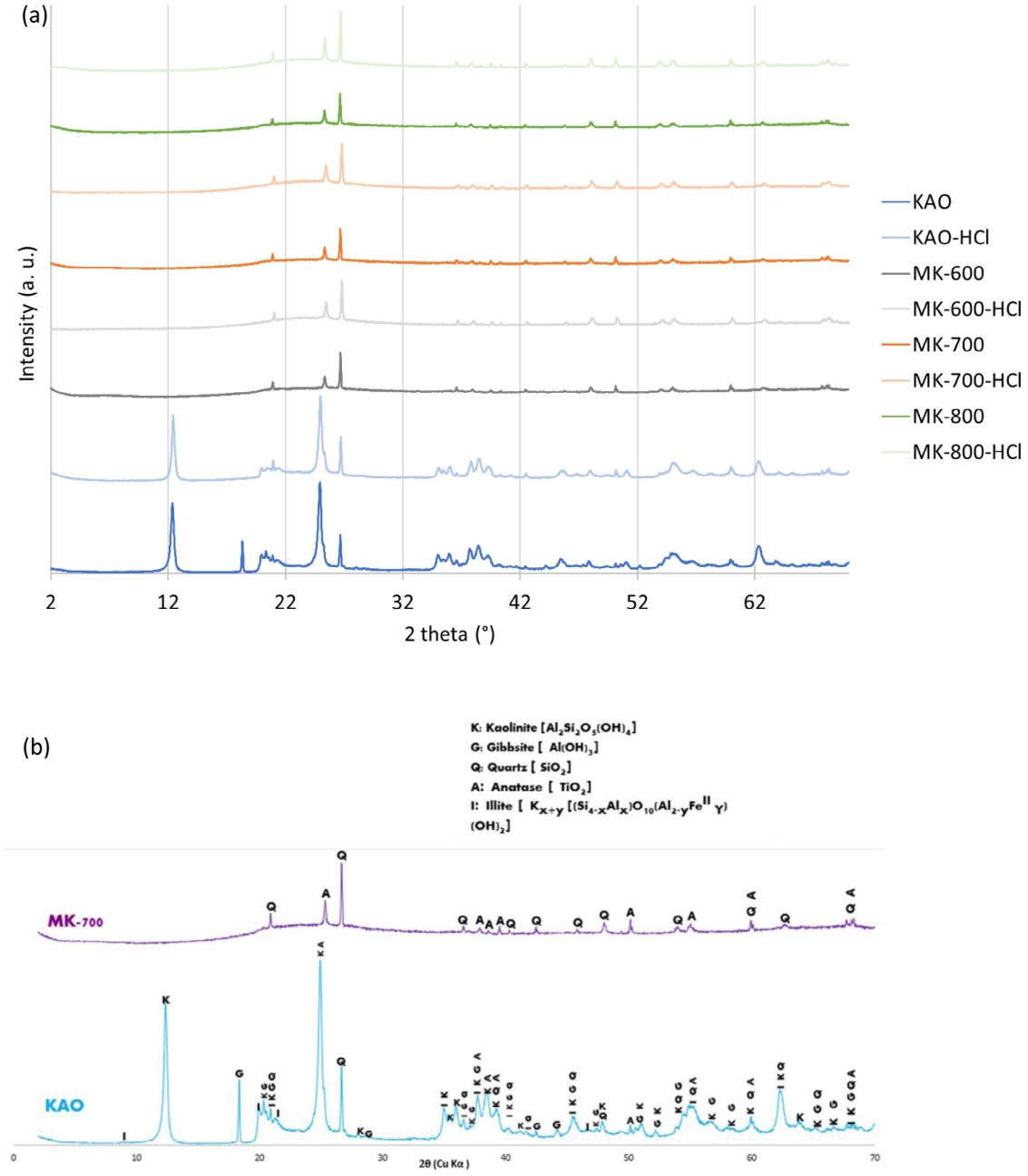


**Fig. 2.** (a) X-ray diffraction (XRD) patterns of all samples and (b) XRD patterns of KAO and MK-700 samples with peak positions as examples.

silicon underwent a relative increase of 43% due to the quantity of amorphous silica generated by the hot acid treatment under reflux conditions. These observations have also been made by other authors (Edama et al., 2014; Yahaya et al., 2017). According to the literature, the resistance of kaolinite to acid leaching is due to the high content of octahedral aluminum (Lenarda et al., 2007; Belver et al., 2002; Yans and Lithostratigraphie, 2007; Mahy et al., 2016; Chmielová and Weiss, 2002; Ptáček et al., 2010; Bich et al., 2009; Panias et al., 2007; Zhou et al., 2021) and also to the sequence of the layers (stacking or structural order) that is determined by abundant hydrogen bonds between the unit layers, which makes acid attack difficult (Torres-Luna and Carriazo, 2019). The loss of protons generated during the dehydroxylation of kaolinite during the heat treatment (600, 700 and 800 °C) can suppress these bonds and destroy the structural order. Thus, the calcination of kaolinite in this work at 800 °C, for example, causes an increase of 16.7% in the concentration in mg/kg of dry matter for aluminum and only 4.7% mg/kg of dry matter for silicon. An increase in the concentration in mg/kg of dry matter for elements such as: Ti, Fe, Mg, P, K and Na was also recorded during the heat treatment at 800 °C of this kaolinite.

The increase in the concentration in mg/kg of dry matter of aluminum and silicon is due to the collapse of the crystal lattice due to the transformation of part of the $AlO_6$ octahedra into much more reactive tetra- and penta-coordinated units (Lenarda et al., 2007; Belver et al., 2002; Yans and Lithostratigraphie, 2007; Mahy et al., 2016; Chmielová and Weiss, 2002; Ptáček et al., 2010; Bich et al., 2009; Panias et al., 2007; Zhou et al., 2021; Jia et al., 2019; Lambert et al., 1989). This increase in concentration is also due to the elimination of hydrogen bonds which reinforce the cohesion between structural units in kaolinite (Torres-Luna and Carriazo, 2019).

However, the hot acid treatment of metakaolinites (kaolinite calcined at 600, 700 and 800 °C) under the same reflux conditions as the previous kaolinite gives results which confirm their greater reactivity compared to natural kaolinite. For the kaolinite calcined at 800 °C

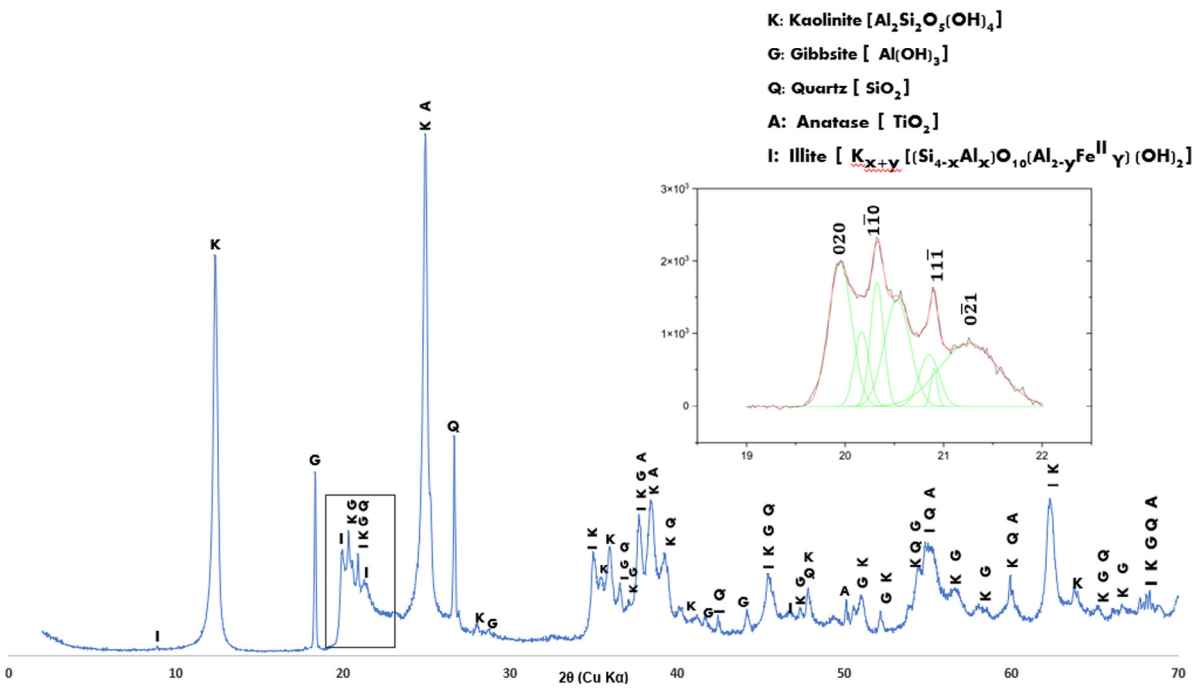


**Fig. 3.** Diffraction analysis of KAO sample and fitting of the 020 and 110 sequences for the determination of the degree of structural disorder.

**Table 1**
Sample chemical composition by inductively coupled plasma–atomic emission spectroscopy (ICP-AES)

| Sample | Al(mg/kg) | Fe(mg/kg) | Mg(mg/kg) | P(mg/kg) | K(mg/kg) | Na(mg/kg) | V(mg/kg) | Si(mg/kg) | Ti(mg/kg) |
|---|---|---|---|---|---|---|---|---|---|
| KAO | 168000 | 6290 | 504 | 4570 | 716 | 3910 | 92 | 130000 | 10700 |
| MK-800 | 196000 | 7630 | 619 | 5080 | 1310 | 4370 | 88 | 136000 | 13300 |
| KAO-HCL | 116000 | 2740 | 320 | 147 | 761 | 118 | 55 | 186000 | 14000 |
| MK-800-HCl | 7770 | 1370 | <50 | 193 | <30 | <50 | <20 | 249000 | 21500 |

(MK-800-HCl), the hot acid treatment caused a 96% drop in the concentration of aluminum and an 83% increase in the concentration of silicon. On the other hand, the concentration of titanium in the MK-800-HCl sample doubled compared to that of natural kaolinite (KAO sample). According to the literature, under reflux conditions the acid treatment causes dissolution of part or most of the $Al^{3+}$ cations of the octahedral sites. It also leads to the formation of an amorphous silica phase (Hai et al., 2015; Liu et al., 2017; Panda et al., 2010; Torres-Luna and Carriazo, 2019; He et al., 2013; Tang et al., 2017; Tao et al., 2014; Bergaya and Lagaly, 2006; Awwad et al., 2022; Aragaw and Alene, 2022; David et al., 2020; Jawad et al., 2022; Selvan et al., 2022; Misra et al., 2022; Zhao et al., 2021; Qu et al., 2017; Ebrahimi et al., 2020; Elimbi et al., 2011; Kenne Diffo et al., 2015; Nmiri, 2017; Reli et al., 2014; Soleimani et al., 2012; Abbassi et al., 2021; Guerra et al., 2012; Ji and Zhang, 2021; Paredes-Quevedo et al., 2021; Lenarda et al., 2007; Belver et al., 2002), which explains the increase in the concentration of silicon matter. However, it should be noted that the elimination of $Al^{3+}$ cations from octahedral sites is greater in metakaolinites than in kaolinite.

### 3.3. Thermal analysis

Fig. 4 presents, respectively, the TGA and DSC profiles for the mother kaolinitic clay (KAO sample), the MK-600 and MK-800 samples, and the thermodifferential analysis (TDA) profile for KAO sample. The TGA, TDA and DSC profiles were recorded during the heating process from 20 to 1200 °C.

From the thermogravimetric analysis of kaolinitic clay (KAO sample), three main mass losses are observed:

(i) The first mass loss of about 0.8% is observed below 150 °C (Fig. 4a). This mass loss is attributed to the elimination of water molecules adsorbed on the external surfaces of the kaolinite particles. Kaolinite has neither intercalated cations nor naturally intercalated water. All the mass losses, in the thermal analysis of kaolinite at this temperature, are thus attributed to the desorption of water. This is also confirmed by the first endothermic peak below 150 °C visible on the TDA curve (Fig. 4c) corresponding to dehydration.

(ii) The second mass loss of about 2.6% is observed around 200 °C or even 300 °C (Fig. 4a). This is attributed to the dehydroxylation of gibbsite (Kenne Diffo et al., 2015; Nmiri, 2017; Reli et al., 2014; Soleimani et al., 2012; Abbassi et al., 2021; Guerra et al., 2012; Ji and Zhang, 2021; Paredes-Quevedo et al., 2021; Lenarda et al., 2007; Belver et al., 2002; Yans and Lithostratigraphie, 2007; Mahy et al., 2016; Chmielová and Weiss, 2002; Ptáček et al., 2010; Bich et al., 2009; Panias et al., 2007; Zhou et al., 2021; Jia et al., 2019; Lambert et al., 1989; Edama et al., 2014; Yahaya et al., 2017; Fabbri et al., 2013). The DSC curve (Fig. 4b) also confirms this with the presence of an endothermic peak centered at 280 °C. On the other hand, between 200 °C and 350 °C, the appearance of an exothermic peak is observed on the TDA curve (Fig. 4c). The latter is linked to the formation of $CO_2$, the product of the complete combustion in the air of the organic carbon present as impurities. The same observations have been made by other authors (Cheng et al., 2010) on Chinese kaolinites.

(iii) The third mass loss of about 11.9% corresponds to the most important thermal reaction observed from 380 °C (Fig. 4a) to around 800 °C. This is attributed to the dehydroxylation of kaolinite and its transformation into metakaolinite (Elimbi et al., 2011; Kenne Diffo et al., 2015; Nmiri, 2017; Reli et al., 2014; Soleimani et al., 2012; Abbassi et al., 2021; Guerra et al., 2012; Ji and Zhang, 2021; Paredes-Quevedo et al., 2021; Lenarda et al., 2007; Belver et al., 2002; Yans and Lithostratigraphie, 2007; Mahy et al., 2016; Chmielová and Weiss, 2002; Ptáček et al., 2010; Bich et al., 2009; Panias et al., 2007; Zhou

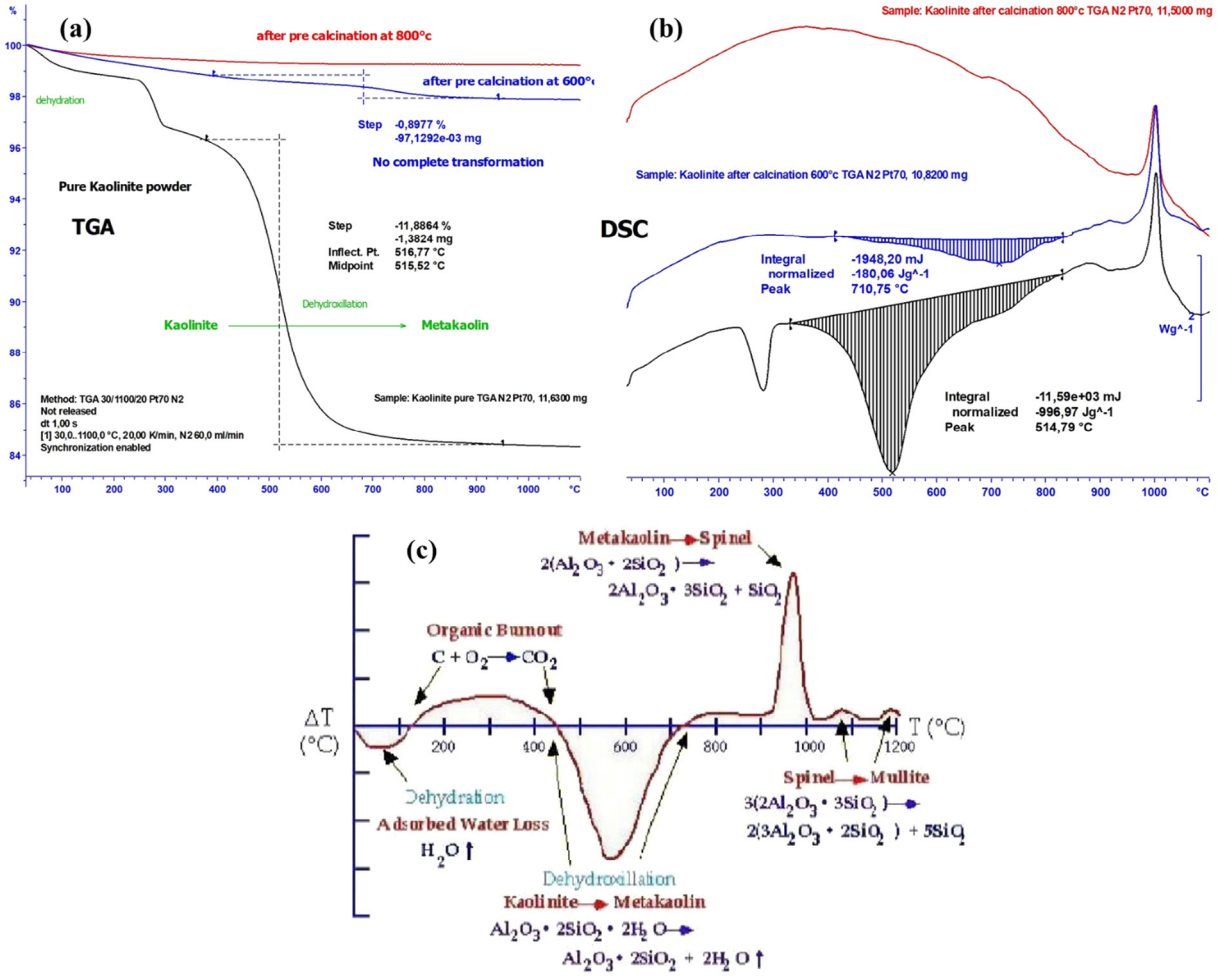


**Fig. 4.** (a) TGA of KAO, MK-600 and MK-800 samples; (b) DSC of KAO, MK-600 and MK-800 samples; and (c) TDA of KAO sample.

et al., 2021; Jia et al., 2019; Lambert et al., 1989; Edama et al., 2014; Yahaya et al., 2017; Fabbri et al., 2013; Cheng et al., 2010; Braccini Freire et al., 2020). This reaction is visible on the DSC and TDA curves with the appearance of an endothermic peak centered around 520 °C (Fig. 4b and c). Considering that the dehydroxylation temperature is influenced by the degree of disorder in the kaolinite structure, the amount and type of impurities, the dehydroxylation observed at a low temperature (380 °C) is consistent with a low Hinckley crystallinity index (1.039) (Cheng et al., 2010).

In the case of metakaolinites, a mass loss of approximately 0.9% is observed below 800 °C on the TGA curve of MK-600. This is attributed to the continuation of the dehydroxylation of kaolinite to obtain metakaolinite (Fig. 4a). On the other hand, the TGA curve of MK-800 (Fig. 4a) shows no mass loss below 800 °C, which suggests that the dehydroxylation of kaolinite at this temperature is complete. From 980 °C, only phase change effects are observed with the appearance of exothermic peaks on the DSC curve (Fig. 4b).

### 3.4. Fourier transform infrared (FTIR) spectral analysis

Fig. 5 presents the FTIR spectra of the kaolinitic clay (KAO sample), those of the metakaolinite samples (MK-600, MK-700 and MK-800) and finally those materials (kaolinite and metakaolinite samples) having undergone an acid treatment. The FTIR spectrum of the KAO sample shows absorption bands at 3689, 3666 and 3618 $cm^{-1}$ characteristic of kaolinite (Torres-Luna and Carriazo, 2019; He et al., 2013; Tang et al., 2017; Tao et al., 2014; Bergaya and Lagaly, 2006; Awwad et al., 2022; Aragaw and Alene, 2022; David et al., 2020; Jawad et al., 2022; Selvan et al., 2022; Misra et al., 2022; Zhao et al., 2021; Qu et al., 2017; Ebrahimi et al., 2020; Elimbi et al., 2011; Kenne Diffo et al., 2015; Diko et al., 2016; Djomgoue and Njopwouo, 2013; Qtaitat and Al-Trawneh, 2005; Saikia and Parthasarathy, 2010). These are the stretch bands of the OH groups coordinated to the octahedral cations (Gao et al., 2016; Hai et al., 2015; Liu et al., 2017; Panda et al., 2010; Torres-Luna and Carriazo, 2019; He et al., 2013; Tang et al., 2017; Tao et al., 2014; Bergaya and Lagaly, 2006; Awwad et al., 2022; Aragaw and Alene, 2022; David et al., 2020; Jawad et al., 2022; Selvan et al., 2022; Misra et al., 2022; Zhao et al., 2021; Qu et al., 2017; Ebrahimi et al., 2020; Elimbi et al., 2011; Kenne Diffo et al., 2015; Nmiri, 2017; Reli et al., 2014; Soleimani et al., 2012; Abbassi et al., 2021; Guerra et al., 2012; Ji and Zhang, 2021; Paredes-Quevedo et al., 2021; Lenarda et al., 2007; Belver et al., 2002; Yans and Lithostratigraphie, 2007; Mahy et al., 2016; Chmielová and Weiss, 2002; Ptáček et al., 2010; Bich et al., 2009; Panias et al., 2007; Zhou et al., 2021; Jia et al., 2019; Lambert et al., 1989; Edama et al., 2014; Yahaya et al., 2017; Fabbri et al., 2013; Cheng et al., 2010; Braccini Freire et al., 2020; Diko et al., 2016; Djomgoue and Njopwouo, 2013; Qtaitat and Al-Trawneh, 2005; Saikia and Parthasarathy, 2010; Dewi et al., 2018). Fig. 5a, b and c show the disappearance of these bands, caused by dehydroxylation, during the calcination of kaolinite at 600, 700 and 800 °C. The bands observed between 1640–3445 $cm^{-1}$ on the FTIR spectra of kaolinite and those of metakaolinites indicate the presence of stretching and deformation vibrations of the OH and H–O–H groups of the absorbed molecules and which are reduced in the FTIR spectra of metakaolinites (MK-X samples) (Elimbi et al., 2011; Kenne Diffo et al., 2015; Nmiri, 2017; Reli et al., 2014; Soleimani et al., 2012; Abbassi et al., 2021; Guerra

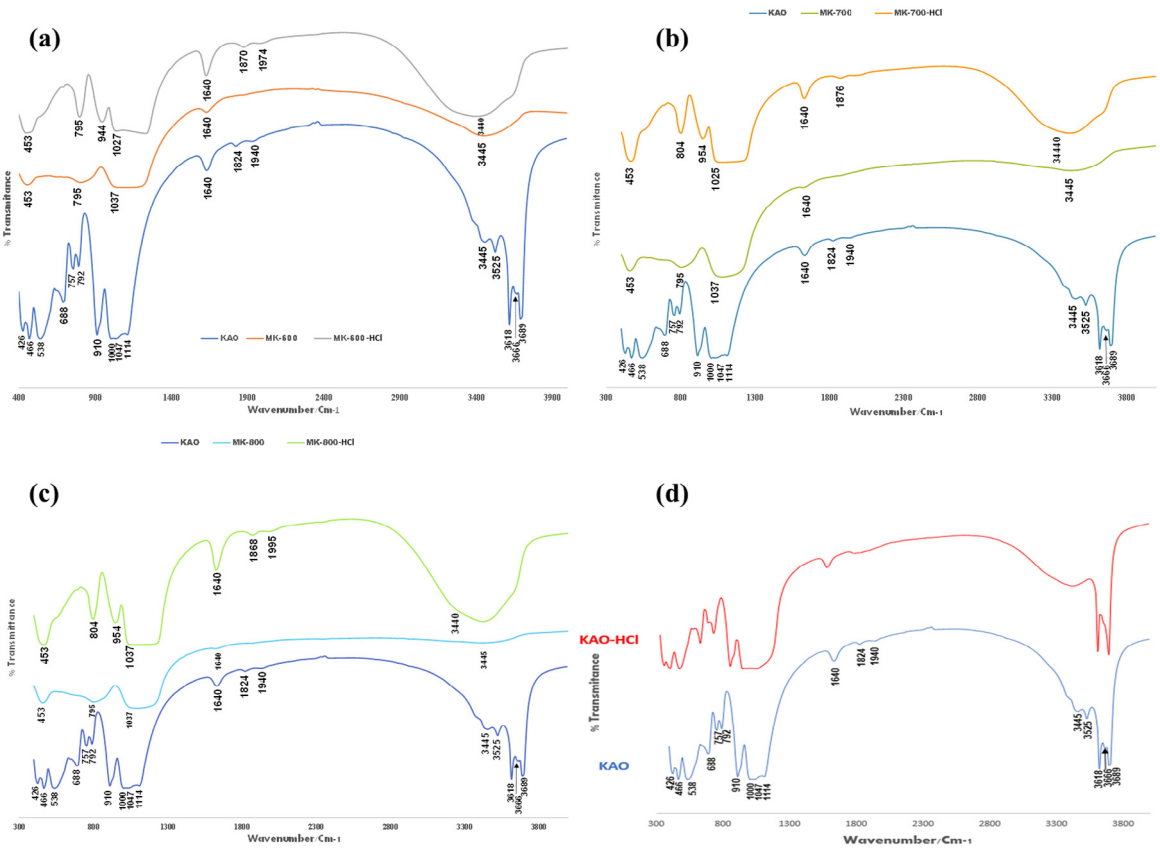


**Fig. 5.** Fourier transform infrared (FTIR) spectra with peak positions of (a) KAO, MK-600 and MK-600-HCl samples; (b) KAO, MK-700 and MK-700-HCl samples; (c) KAO, MK-800 and MK-800-HCl samples; and (d) KAO and KAO-HCl samples.

et al., 2012; Ji and Zhang, 2021; Paredes-Quevedo et al., 2021; Lenarda et al., 2007; Belver et al., 2002; Yans and Lithostratigraphie, 2007; Mahy et al., 2016; Chmielová and Weiss, 2002; Ptáček et al., 2010; Bich et al., 2009; Panias et al., 2007; Zhou et al., 2021; Jia et al., 2019; Lambert et al., 1989; Edama et al., 2014; Yahaya et al., 2017; Fabbri et al., 2013; Cheng et al., 2010; Braccini Freire et al., 2020; Diko et al., 2016; Djomgoue and Njopwouo, 2013; Qtaitat and Al-Trawneh, 2005; Saikia and Parthasarathy, 2010). The bands observed at 1114, 1047 and 1016 $cm^{-1}$ on the FTIR spectrum of kaolinite (KAO sample) correspond respectively to the deformation vibrations of the Si–O, Si–O–Si and Si–O–Al bonds (Kenne Diffo et al., 2015; Nmiri, 2017; Reli et al., 2014; Soleimani et al., 2012; Abbassi et al., 2021; Guerra et al., 2012; Ji and Zhang, 2021; Paredes-Quevedo et al., 2021; Lenarda et al., 2007; Belver et al., 2002; Yans and Lithostratigraphie, 2007; Mahy et al., 2016; Chmielová and Weiss, 2002; Ptáček et al., 2010; Bich et al., 2009; Panias et al., 2007; Zhou et al., 2021). However, after the calcination of kaolinite at 600, 700 and 800 °C, the transformation of the latter into metakaolinite is confirmed by the disappearance of these absorption bands and the appearance of a wide band around 1037 $cm^{-1}$ reflecting the presence of asymmetric and symmetrical stretching vibrations of the Si–O–Al and Si–O–Si bonds (Tironi et al., 2012). Two bands on the FTIR spectrum of kaolinite (KAO sample): one at 3525 $cm^{-1}$ and the other at 910 $cm^{-1}$ are related to Al(VI)–OH and Al(VI)–O stretching vibrations, respectively. The development of these bands has also been observed between 400–1000 $cm^{-1}$ for the Al–O bond and between 3100–3600 $cm^{-1}$ for the Al–OH bond in the case of gibbsite (Kiani et al., 2016). After the calcination of kaolinite at 600, 700 and 800 °C, these bands disappear and the coordination vibration IV of Al(IV)–O appears as a wide band around 795 $cm^{-1}$ (Soleimani et al., 2012). The other bands of no less importance on the FTIR spectrum of kaolinite are at 792 $cm^{-1}$ (free silica and/or quartz always present in natural samples), 757 $cm^{-1}$ (Si–O–Al), 688 $cm^{-1}$ (Si–O out-of-plane bending), 538 $cm^{-1}$ (Si–O–Al octahedral Al bending), 466 $cm^{-1}$ (Si–O–Si in-plane bending) and 426 $cm^{-1}$ (Si–O) (Diko et al., 2016; Djomgoue and Njopwouo, 2013; Qtaitat and Al-Trawneh, 2005; Saikia and Parthasarathy, 2010).

Fig. 5d shows the FTIR spectrum of kaolinite having undergone the hot acid treatment (KAO-HCl sample). In comparison with the spectrum of the KAO sample, it is clear that under these conditions kaolinite develops very high resistance to acid leaching since the absorption bands at 3689, 3666 and 3618 $cm^{-1}$ (attributed to the vibration stretching of OH groups coordinated to $Al^{3+}$ cations) remained intact. This result is consistent with the XRD analysis (Fig. 2). Other authors (Gao et al., 2016; Hai et al., 2015; Liu et al., 2017; Panda et al., 2010; Torres-Luna and Carriazo, 2019; He et al., 2013; Tang et al., 2017; Tao et al., 2014; Bergaya and Lagaly, 2006; Awwad et al., 2022; Aragaw and Alene, 2022; David et al., 2020; Jawad et al., 2022; Selvan et al., 2022; Misra et al., 2022; Zhao et al., 2021; Qu et al., 2017; Ebrahimi et al., 2020; Elimbi et al., 2011; Kenne Diffo et al., 2015; Nmiri, 2017; Reli et al., 2014; Soleimani et al., 2012; Abbassi et al., 2021; Guerra et al., 2012; Ji and Zhang, 2021; Paredes-Quevedo et al., 2021; Lenarda et al., 2007; Belver et al., 2002; Yans and Lithostratigraphie, 2007; Mahy et al., 2016; Chmielová and Weiss, 2002; Ptáček et al., 2010; Bich et al., 2009; Panias et al., 2007; Zhou et al., 2021) came to the same conclusions with Chinese kaolinites heat-treated (up to 200 °C) with concentrated sulfuric acid. In the present case, the disappearance of the absorption band at 3525 $cm^{-1}$ is due to the attack on the aluminum of the Al–OH groups of the gibbsite present as an impurity in this clay.

The FTIR spectra of metakaolinites treated with hot concentrated HCl are also presented in Fig. 5a, b and c. A broad band is observed around 3440 $cm^{-1}$. The intensity of this band increases with the temperature of calcination. It is attributed to the high amount of water physi-sorbed on the surface of the generated amorphous silica (Lenarda et al., 2007; Belver et al., 2002; Yans and Lithostratigraphie, 2007;

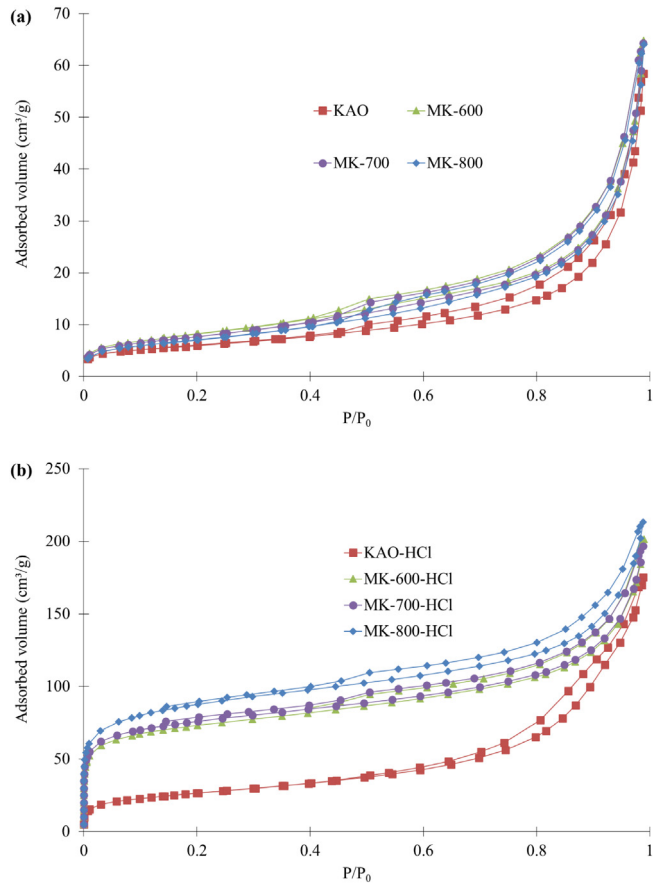


**Fig. 6.** Nitrogen adsorption–desorption isotherms for (a) KAO and heated samples and (b) acid treated samples.

Mahy et al., 2016; Chmielová and Weiss, 2002; Ptáček et al., 2010; Bich et al., 2009; Panias et al., 2007; Zhou et al., 2021; Jia et al., 2019; Lambert et al., 1989; Edama et al., 2014; Yahaya et al., 2017; Fabbri et al., 2013; Cheng et al., 2010; Braccini Freire et al., 2020; Diko et al., 2016; Djomgoue and Njopwouo, 2013; Qtaitat and Al-Trawneh, 2005; Saikia and Parthasarathy, 2010; Dewi et al., 2018; Tironi et al., 2012; Kiani et al., 2016; Vicente-Rodriguez et al., 1996). The curvature band of these water molecules is also observed at 1640 $cm^{-1}$. This broad band was also found around 3400 $cm^{-1}$ after acid activation of a commercial kaolinite calcined at 700 and 900 °C (Torres-Luna and Carriazo, 2019). The authors attributed the latter to the vibration of SiO–H bonds in silica-rich solids as a result of a dealumination reaction. However, in Fig. 5a, b and c, the bands corresponding to silica could be observed between 1300 and 400 $cm^{-1}$: the stretching band of Si–O–Si at 1037 $cm^{-1}$, at 804–954 $cm^{-1}$ with unaltered free silica and/or quartz, and finally the Si–O–Si bending vibration at 453 $cm^{-1}$.

### 3.5. Textural analysis

Fig. 6 shows the nitrogen adsorption–desorption isotherms of kaolinite and metakaolinite samples as well as those of the solids having undergone hot acid treatment. The specific surface area and pore volume values of all materials are listed in Table 2.

The nitrogen adsorption–desorption isotherm of natural kaolinitic clay (KAO sample, Fig. 6a) corresponds to a type II of the IUPAC classification system (Thommes et al., 2015). The specific surface area of this solid is equal to 20 $m^2/g$. The shape of the isotherm and the surface are typical of natural kaolinites, as reported by Thommes et al. (2015). This is characteristic of macroporous adsorbents because at high pressure the adsorbed volume increases rapidly. After the heat treatment at 600, 700 and 800 °C (Fig. 6a), the shape of the isotherm did not change, and the specific surface areas increased slightly as shown in Table 2. This slight increase is related to the elimination, by the heat treatment, of the organic matter present as impurities at the level of the interfoliar spaces, in agreement with the TDA results. Despite this small increase in the BET surfaces of the solids after heat treatment, the contribution of the micropores to the specific surface area remains negligible (Table 2). Other authors (Torres-Luna and Carriazo, 2019) came to the same conclusion with a commercial natural kaolinite calcined for 2 h at 700 and 900 °C. It should be observed here that the hysteresis on the adsorption–desorption isotherms of the metakaolinite samples (MK-600, MK-700 and MK-800) tend to become asymptotic at relative pressures close to 1 (Fig. 6a). These also end in a stair at low relative pressures, and are characteristic of capillary condensation in small mesopores.

However, the hot acid treatment (110 °C) of natural kaolinite and metakaolinites affected the behavior of the isotherms (Fig. 6b). The acid attack of kaolinite and metakaolinites has modified the mesoporous surfaces. An increase in the mesoporous surface is observed in the clay materials; it is more intense with the increasing temperature of calcination (Table 2). The nitrogen adsorption–desorption isotherms of metakaolinites treated with hot acid show a strong increase in the adsorbed volume at very low relative pressures. This increase is followed by a plateau, corresponding to the type IV isotherm (Thommes et al., 2015) of the IUPAC classification and which is characteristic of microporous adsorbents. The acid treatment of metakaolinites gives rise to highly microporous materials. The values of the microporous surfaces ($S_{micro}$, Table 2) range between 125 $m^2/g$ for MK-600-HCl, 130 $m^2/g$ for MK-700-HCl and 140 $m^2/g$ for MK-800-HCl. The values of the BET surfaces ($S_{BET}$, Table 2) increased from 255 $m^2/g$ for MK-600-HCl, 275 $m^2/g$ for MK-700-HCl to 315 $m^2/g$ for MK-800-HCl. Similarly, in these isotherms, the hysteresis loops are narrow for relative pressure values close to 1. This is characteristic of capillary condensation in large mesopores. The KAO-HCl, MK-600-HCl, MK-700-HCl and MK-800-HCl materials have developed microporosity and mesoporosity with greater microporosity and mesoporosity in the solids MK-600-HCl, MK-700-HCl and MK-800-HCl compared to KAO-HCl sample (Table 2).

### 3.6. Morphology

Fig. 7 presents the SEM micrographs of kaolinite, metakaolinites, and kaolinite and metakaolinites having undergone the acid treatment. These micrographs confirm the different textures of the materials with different surface values. One can observe the morphology of kaolinite (Fig. 7a) that is typically two-dimensional (Tang et al., 2017; Tao et al., 2014; Bergaya and Lagaly, 2006; Awwad et al., 2022; Aragaw and Alene, 2022; David et al., 2020; Jawad et al., 2022; Selvan et al., 2022; Misra et al., 2022; Zhao et al., 2021; Qu et al., 2017; Ebrahimi et al., 2020; Elimbi et al., 2011; Kenne Diffo et al., 2015; Nmiri, 2017; Reli et al., 2014; Soleimani et al., 2012; Abbassi et al., 2021; Guerra et al., 2012; Ji and Zhang, 2021; Paredes-Quevedo et al., 2021; Lenarda et al., 2007; Belver et al., 2002; Yans and Lithostratigraphie, 2007; Mahy et al., 2016; Chmielová and Weiss, 2002; Ptáček et al., 2010; Bich et al., 2009; Panias et al., 2007; Zhou et al., 2021) characterized by pseudo-hexagonal stacking (Zhou et al., 2014) of platelets on top of each other. The presence of needles (Fig. 7a) is related to the degree of disorder in its structure. After calcination at 600, 700 and 800 °C (Fig. 7c, e, and g), the transformation of the kaolinite into metakaolinite caused thinning due to reduction in the thickness or distance between the plates (or sheets) (Ptáček et al., 2010). The decrease in the distance between the platelets is probably caused by the elimination of structural water molecules during the heat treatment.

Moreover, it is observed that the morphology of the metakaolinite samples having undergone acid treatment (Fig. 7d, f, and h) is characterized by a rough and spongy texture. Such texture is a characteristic

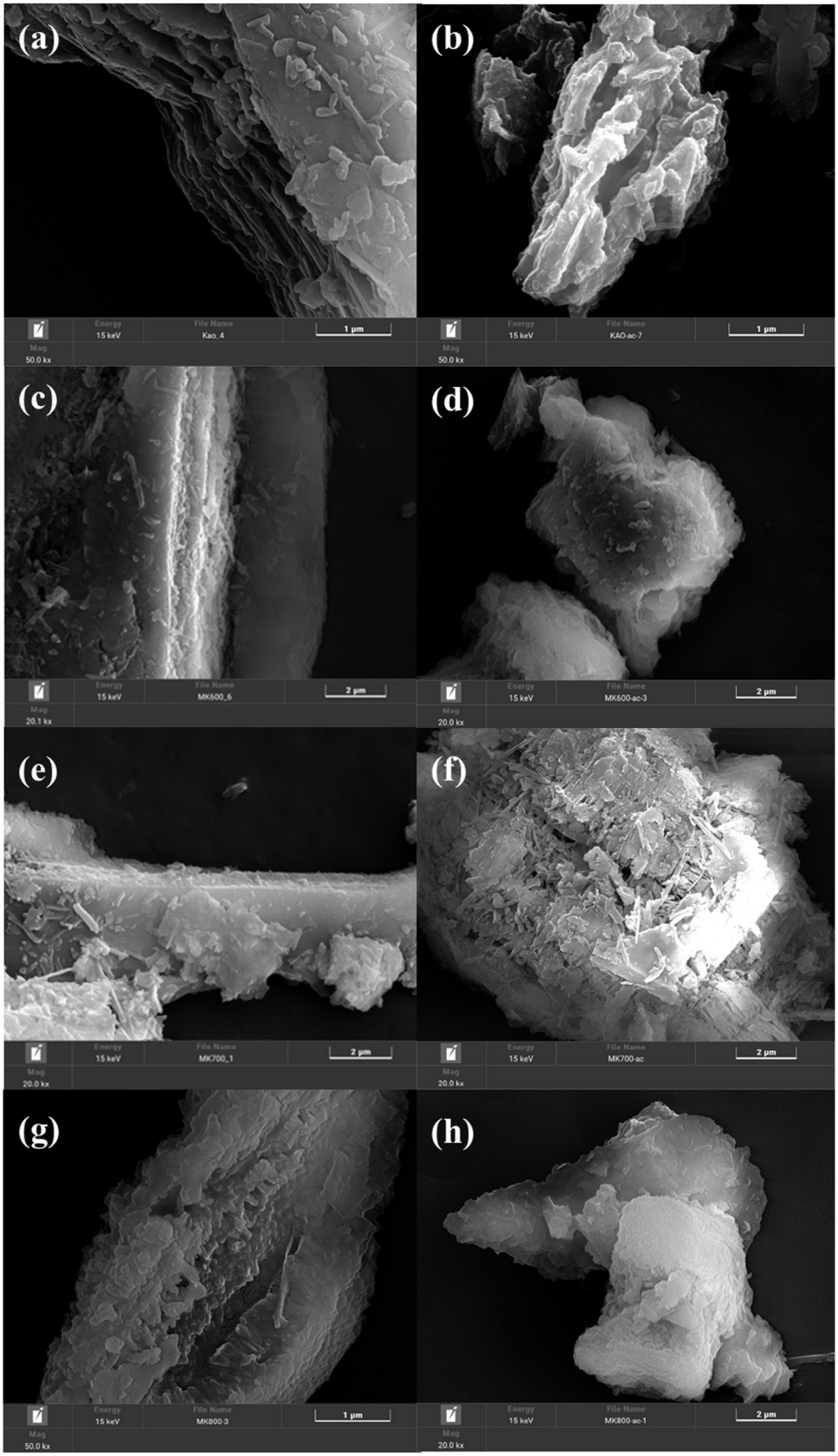


**Fig. 7.** Scanning electron microscope (SEM) micrographs of (a) KAO, (b) KAO-HCl, (c) MK-600, (d) MK-600-HCl, (e) MK-700, (f) MK-700-HCl, (g) MK-800, and (h) MK-800-HCl samples.

**Table 2**
Sample textural properties.

| Sample | $S_{BET}$ ($m^2/g$) ±5 | $S_{meso}$ ($m^2/g$) ±5 | $S_{micro}$ ($m^2/g$) ±5 | $V_T$ ($cm^3/g$) ±0.01 | $V_{meso}$ ($cm^3/g$) ±0.01 | $V_{micro}$ ($cm^3/g$) ±0.01 |
|---|---|---|---|---|---|---|
| KAO | 20 | 15 | 5 | 0.09 | 0.08 | 0.01 |
| MK-600 | 30 | 25 | 5 | 0.10 | 0.08 | 0.02 |
| MK-700 | 30 | 25 | 5 | 0.10 | 0.08 | 0.02 |
| MK-800 | 25 | 20 | 5 | 0.10 | 0.08 | 0.02 |
| KAO-HCl | 95 | 80 | 15 | 0.27 | 0.22 | 0.05 |
| MK-600-HCl | 255 | 130 | 125 | 0.30 | 0.19 | 0.11 |
| MK-700-HCl | 275 | 145 | 130 | 0.30 | 0.19 | 0.11 |
| MK-800-HCl | 315 | 175 | 140 | 0.33 | 0.20 | 0.13 |

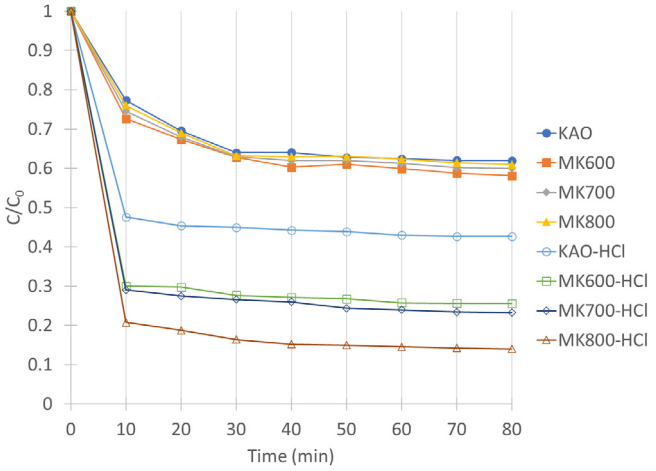


**Fig. 8.** C/C evolution over time for 100 mg concentrations of powder samples for the 8 clays.

form of very porous solids in accordance with the high specific surface area of these materials (Lenarda et al., 2007; Belver et al., 2002). Also, during the acid treatment of natural kaolinite (Fig. 7d, f, and h), the relatively smooth surface of the latter becomes rough. The stacking of particles which initially are in a two-dimensional structure are moving towards a narrower three-dimensional structure (Tang et al., 2017; Tao et al., 2014; Bergaya and Lagaly, 2006; Awwad et al., 2022; Aragaw and Alene, 2022; David et al., 2020; Jawad et al., 2022; Selvan et al., 2022; Misra et al., 2022; Zhao et al., 2021; Qu et al., 2017; Ebrahimi et al., 2020; Elimbi et al., 2011; Kenne Diffo et al., 2015; Nmiri, 2017; Reli et al., 2014; Soleimani et al., 2012; Abbassi et al., 2021; Guerra et al., 2012; Ji and Zhang, 2021; Paredes-Quevedo et al., 2021; Lenarda et al., 2007; Belver et al., 2002; Yans and Lithostratigraphie, 2007; Mahy et al., 2016; Chmielová and Weiss, 2002; Ptáček et al., 2010; Bich et al., 2009; Panias et al., 2007; Zhou et al., 2021). This structural change is explained by the partial collapse of the crystalline structure.

### *3.7. Adsorption of malachite green (MG)*

The evolution of MG concentration over time by adsorption on the 8 samples is represented in Fig. 8. It is observed that KAO, MK600, MK700 and MK800 samples have similar adsorption properties with 40% of MG adsorbed after 80 min. KAO-HCl has a higher adsorption of 55% of MG, MK600-HCl and MK700-HCl around 70%, and finally MK800-HCl has the highest adsorption rate with 85% of MG adsorbed. The evolution of the adsorption follows the $S_{BET}$ value of the samples. The highest specific surface area leads to the best adsorption. The combination of calcination at 800 °C followed by the HCl treatment allows the adsorption of MG to double between KAO and MK800-HCl samples.

Table 3 compares this work to the literature concerning the treatment of clays to modify their physicochemical properties and their uses in environmental applications. A direct comparison is not easy due to many parameters that differ across the studies, such as the composition of the clays, the treatment temperature, the concentration of acid or base, and the various conditions for the adsorption experiments. Table 3 summarizes the type of materials, the treatment applied, and the main results for the adsorption properties (the pollutant or adsorption capacity) or the specific surface area obtained. It is observed that the materials of this present study reach a very high specific surface area up to 315 $m^2/g$. The study of Paredes-Quevedo et al. (2021) has a higher specific surface area (up to 594 $m^2/g$) but with a high calcination temperature and the adsorption is evaluated using another model pollutant, basic red 46. The study of Shayesteh et al. (2015) uses MG as pollutant for the adsorption experiment but a different kind of natural material is used as adsorbent, pumice stone. This material is less porous than clay but can adsorb MG if a higher adsorbent dose is used. In Belver et al. (2002), a similar treatment to this study is used but a lower specific surface area is obtained (up to 219 $m^2/g$) and the adsorption is not evaluated.

In this study, optimized acidic and thermal conditions are determined to obtain highly porous materials with promising adsorption properties.

## 4. Conclusions

In this work, a natural kaolinitic clay mineral from Kribi in Cameroon is modified by thermal and acidic treatments. The influence of these treatments is studied on the physicochemical properties of the clay materials. Three calcination temperatures are explored: 600, 700 and 800 °C. Acidic treatment is applied on the untreated and heated clays, leading to a total of 8 samples that are characterized using various techniques.

The XRD pattern of the untreated clay showed that the mineral is composed of kaolinite. Calcination at temperatures of 600, 700 and 800 °C allowed amorphization of the natural kaolinitic clay to obtain metakaolinite which is a more reactive material and whose structure is more sensitive to acidic treatment. This prior heat treatment of the natural clay produces dehydroxylation and disintegration by rupture of the strong hydrogen bonds between the layers of the clay. Heat treatment did not increase the specific surface area of the clay, which stayed around 20–30 $m^2/g$.

When acid treatment is applied, it produces a high material texture modification giving microporous materials with a large surface area up to 315 $m^2/g$ with the sample previously calcined at 800 °C. This treatment also allowed a significant increase in mesoporosity in these materials. The microporosity and mesoporosity increase is greater when the clay is calcined at higher temperature.

The morphology of the samples (observed by SEM) is modified when acidic treatment is applied. The stacking of particles, which initially are in a two-dimensional structure, moves towards a narrower three-dimensional porous structure.

First preliminary adsorption experiments showed that these modified clays can effectively adsorb a model pollutant, malachite green. The best-performing sample can adsorb 85 mg/L of MG in 80 min of contact time. These treatments open the way to produce highly porous clay materials that could be used as adsorbent materials for pollutant removal in water.

**Table 3**
Comparison to some studies in the literature.

| References | Type of material | Treatment applied | Main results |
|---|---|---|---|
| This work | Natural kaolinitic clay from Cameroon (Kirby) | Heat treatment (600, 700 and 800 °C)<br>Acidic treatment (6 M HCl at 110 °C) | Highly porous metakaolinite (up to 315 $m^2/g$)<br>Adsorption of MG (80 mg/L in 10 min) |
| Hamdi and Srasra (2012) | Tunisian kaolinitic/smectic clays and synthetic zeolites | Washed and dried at 80 °C | Phosphate ion adsorption<br>Porous clays (up to 106 $m^2/g$) |
| Nodehi et al. (2020) | Natural clinoptilolite from Iran | Washed and dried at 80 °C + surfactant treatment (hexadecyltrimethylammonium bromide cationic surfactant) | Congo red adsorption (up to 200 mg of CR/g of material)<br>Low porous materials (up to 12 $m^2/g$) |
| Shayesteh et al. (2015) | Pumice stone from Iran | Washed and dried at 80 °C | Malachite green and crystal violet adsorption (22.57 mg/g and 6.99 mg/g of adsorption capacity)<br>Low porous materials (up to 7 $m^2/g$) |
| Tchanang et al. (2021) | Kaolinitic clay from Cameroon (Dibamba) | Heat treatment (600, 700 and 800 °C)<br>Acidic (2.5. M of HCl or $H_2SO_4$ or $HNO_3$) or basic treatment (2 M of NaOH or KOH) | Porous materials (up to 80 $m^2/g$) for methylene blue adsorption (99.9% adsorption capacity) |
| Paredes-Quevedo et al. (2021) | Colombian clay | Heat treatment (700 and 900 °C)<br>Acidic treatment (3 M HCl at 90 °C) | Basic red 46 adsorption (100% in 20 min)<br>Highly porous materials (up to 594 $m^2/g$) |
| Lenarda et al. (2007) | Kaolin from Aldrich | Heat treatment (850 and 950 °C)<br>Acidic treatment (1 M $H_2SO_4$ at 90 °C) | Catalytic 1-butene isomerization tests<br>Porous materials (up to 288 $m^2/g$) |
| Belver et al. (2002) | Spanish kaolin | Heat treatment (600, 700, 800 and 900 °C)<br>Acidic (6 M of HCl at 90 °C) or basic treatment (1-5 M of KOH at 25 °C) | Porous materials (up to 219 $m^2/g$) |

## CRediT authorship contribution statement

**Pierre Ngue Song:** Conceptualization, Methodology, Writing – original draft, Writing – review & editing, Investigation, Formal analysis. **Julien G. Mahy:** Methodology, Formal analysis, Writing – original draft, Writing – review & editing, Supervision. **Cédric Calberg:** Investigation, Methodology, Formal analysis, Writing – review & editing. **Antoine Farcy:** Investigation, Formal analysis, Writing – review & editing. **Joachim Caucheteux:** Investigation, Formal analysis, Writing – review & editing. **Nathalie Fagel:** Conceptualization, Methodology, Writing – review & editing, Supervision, Funding acquisition, Project administration. **Stéphanie D. Lambert:** Conceptualization, Methodology, Formal analysis, Writing – review & editing, Funding acquisition, Project administration, Supervision.

## Declaration of competing interest

The authors declare that they have no known competing financial interests or personal relationships that could have appeared to influence the work reported in this paper.

## Data availability

Data will be made available on request

## Acknowledgments

The authors acknowledge Joel Otten and Nicolas Delmelle for their technical support. Julien G. Mahy and Stéphanie D. Lambert thank the F.R.S.-FNRS for their Postdoctoral Researcher position and Research Director position, respectively. J.G.M. is grateful to the Rotary for a District 2160 grant, to the University of Liège and the FNRS for financial support for a postdoctoral stay at INRS Centre Eau, Terre, Environnement in Québec, Canada.

## References

Abbassi, H., Abidi, R., Memia, Zayani, B., 2021. A short review on the silylated clays-polymer nanocomposites: Synthesis, properties and applications. J. Marocain de Chim. Hétérocyclique Moroccan J. Heterocyclic Chem. J. Mar. Chim. Heterocycl. 20, 117–134.

Aragaw, T.A., Alene, A.N., 2022. A comparative study of acidic, basic, and reactive dyes adsorption from aqueous solution onto kaolin adsorbent: Effect of operating parameters, isotherms, kinetics, and thermodynamics. Emerg. Contam. 8, 59–74. http://dx.doi.org/10.1016/j.emcon.2022.01.002.

Awwad, A.M., Amer, M.W., Al-aqarbeh, M.M., 2022. TiO2-kaolinite nanocomposite prepared from the Jordanian Kaolin clay: Adsorption and thermodynamicsof Pb(II) and Cd(II) ions in aqueous solution. Chem. Int. 6, 168–178.

Belver, C., Bañares Muñoz, M.A., Vicente, M.A., 2002. Chemical activation of a kaolinite under acid and alkaline conditions. Chem. Mater. 14, 2033–2043. http://dx.doi.org/10.1021/cm0111736.

Bergaya, F., Lagaly, G., 2006. Chapter 1 general introduction: Clays, clay minerals, and clay science. In: Bergaya, F., Theng, B.K.G., Lagaly, G. (Eds.), Handbook of Clay Science. Elsevier, pp. 1–18. http://dx.doi.org/10.1016/S1572-4352(05)01001-9.

Bich, C., Ambroise, J., Péra, J., 2009. Influence of degree of dehydroxylation on the pozzolanic activity of metakaolin. Appl. Clay Sci. 44, 194–200. http://dx.doi.org/10.1016/j.clay.2009.01.014.

Braccini Freire, C., Lourencio Dias dos Santos, B., Lobo Filgueiras de Miranda, I., Avellar Rodrigues, M., Soares Lameiras, F., 2020. Influence of the kaolinite calcination conditions on the compressive strength of geopolymer. KnE Eng. http://dx.doi.org/10.18502/keg.v5i4.6790.

Cheng, H., Yang, J., Liu, Q., He, J., Frost, R.L., 2010. Thermogravimetric analysis-mass spectrometry (TG-MS) of selected Chinese kaolinites. Thermochim Acta. 507–508, 106–114. http://dx.doi.org/10.1016/j.tca.2010.05.007.

Chmielová, M., Weiss, Z., 2002. Determination of structural disorder degree using an XRD profile fitting procedure. Application to Czech kaolins. Appl. Clay Sci. 22, 65–74, www.elsevier.com/locate/clay.

David, M.K., Okoro, U.C., Akpomie, K.G., Okey, C., Oluwasola, H.O., 2020. Thermal and hydrothermal alkaline modification of kaolin for the adsorptive removal of lead(II) ions from aqueous solution. SN Appl. Sci. 2, http://dx.doi.org/10.1007/s42452-020-2621-7.

Dewi, R., Agusnar, H., Alfian, Z., Tamrin, 2018. Characterization of technical kaolin using XRF, SEM, XRD, FTIR and its potentials as industrial raw materials. J. Phys. Conf. Ser., Institute of Physics Publishing http://dx.doi.org/10.1088/1742-6596/1116/4/042010.

Diko, M., Ekosse, G., Ogola, J., 2016. Fourier transform infrared spectroscopy and thermal analyses of kaolinitic clays from south africa and Cameroon. Acta Geodyn. et Geomater. 13, 149–158. http://dx.doi.org/10.13168/AGG.2015.0052.

Djomgoue, P., Njopwouo, D., 2013. FT-IR spectroscopy applied for surface clays characterization. J. Surf. Eng. Mater. Adv. Technol. 03, 275–282. http://dx.doi.org/10.4236/jsemat.2013.34037.

Dong, J., Zhang, J., 2018. Biomimetic super anti-wetting coatings from natural materials: Superamphiphobic coatings based on nanoclays. Sci. Rep. 8, http://dx.doi.org/10.1038/s41598-018-30586-4.

Ebrahimi, A., Haghighi, M., Aghamohammadi, S., 2020. Effect of calcination temperature and composition on the spray-dried microencapsulated nanostructured SAPO-34 with kaolin for methanol conversion to ethylene and propylene in fluidized bed reactor. Microporous Mesoporous Mater. 297, http://dx.doi.org/10.1016/j.micromeso.2020.110046.

Edama, N.A., Sulaiman, A., Ku Hamid, K.H., Rodhi, M.N.M., Musa, M., Rahim, S.N.A., 2014. The effect of hydrochloric acid on the surface area, morphology and physicochemical properties of sayong kaolinite clay. In: Key Eng Mater. Trans Tech Publications Ltd, pp. 49–56. http://dx.doi.org/10.4028/www.scientific.net/KEM.594-595.49.

Elimbi, A., Tchakoute, H.K., Njopwouo, D., 2011. Effects of calcination temperature of kaolinite clays on the properties of geopolymer cements. Constr. Build. Mater. 25, 2805–2812. http://dx.doi.org/10.1016/j.conbuildmat.2010.12.055.

Fabbri, B., Gualtieri, S., Leonardi, C., 2013. Modifications induced by the thermal treatment of kaolin and determination of reactivity of metakaolin. Appl. Clay Sci. 73, 2–10. http://dx.doi.org/10.1016/j.clay.2012.09.019.

Gao, W., Zhao, S., Wu, H., Deligeer, W., Asuha, S., 2016. Direct acid activation of kaolinite and its effects on the adsorption of methylene blue. Appl. Clay Sci. 126, 98–106. http://dx.doi.org/10.1016/j.clay.2016.03.006.

Guerra, D.L., Oliveira, S.P., Silva, R.A.S., Silva, E.M., Batista, A.C., 2012. Dielectric properties of organofunctionalized kaolinite clay and application in adsorption mercury cation. Ceram. Int. 38, 1687–1696. http://dx.doi.org/10.1016/j.ceramint.2011.09.062.

Hai, Y., Li, X., Wu, H., Zhao, S., Deligeer, W., Asuha, S., 2015. Modification of acid-activated kaolinite with TiO2 and its use for the removal of azo dyes. Appl. Clay Sci. 114, 558–567. http://dx.doi.org/10.1016/j.clay.2015.07.010.

Hamdi, N., Srasra, E., 2012. Removal of phosphate ions from aqueous solution using Tunisian clays minerals and synthetic zeolite. J. Environ. Sci. 24, 617–623. http://dx.doi.org/10.1016/S1001-0742(11)60791-2.

He, H., Tao, Q., Zhu, J., Yuan, P., Shen, W., Yang, S., 2013. Silylation of clay mineral surfaces. Appl. Clay Sci. 71, 15–20. http://dx.doi.org/10.1016/j.clay.2012.09.028.

Jawad, A.H., Abdulhameed, A.S., Kashi, E., Yaseen, Z.M., ALOthman, Z.A., Khan, M.R., 2022. Cross-linked chitosan-glyoxal/kaolin clay composite: Parametric optimization for color removal and COD reduction of remazol brilliant blue R dye. J. Polym. Environ. 30, 164–178. http://dx.doi.org/10.1007/s10924-021-02188-1.

Ji, B., Zhang, W., 2021. Rare earth elements (REEs) recovery and porous silica preparation from kaolinite. Powder Technol. 391, 522–531. http://dx.doi.org/10.1016/j.powtec.2021.06.028.

Jia, X., Cheng, H., Zhou, Y., Zhang, S., Liu, Q., 2019. Time-efficient preparation and mechanism of methoxy-grafted kaolinite via acid treatment and heating. Appl. Clay Sci. 174, 170–177. http://dx.doi.org/10.1016/j.clay.2019.04.001.

Kenne Diffo, B.B., Elimbi, A., Cyr, M., Dika Manga, J., Tchakoute Kouamo, H., 2015. Effect of the rate of calcination of kaolin on the properties of metakaolin-based geopolymers. J. Asian Ceramic Soc. 3, 130–138. http://dx.doi.org/10.1016/j.jascer.2014.12.003.

Kiani, S., Mansouri Zadeh, M., Khodabakhshi, S., Rashidi, A., Moghadasi, J., 2016. Newly prepared nano Gamma alumina and its application in enhanced oil recovery: An approach to low-salinity waterflooding. Energy Fuels 30, 3791–3797. http://dx.doi.org/10.1021/acs.energyfuels.5b03008.

Lambert, J.F., Millman, W.S., Fripiat, J.J., 1989. Revisiting kaolinite dehydroxylation: A 29Si and 27Al MAS NMR study. J. Am. Soc. 111, 3517–3522.

Lenarda, M., Storaro, L., Talon, A., Moretti, E., Riello, P., 2007. Solid acid catalysts from clays: Preparation of mesoporous catalysts by chemical activation of metakaolin under acid conditions. J. Colloid Interface Sci. 311, 537–543. http://dx.doi.org/10.1016/j.jcis.2007.03.015.

Liu, S.X., Xue, C., Yang, H., Huang, X.Q., Zou, Y., Ding, Y.N., Li, L., Ren, X.M., 2017. Intercalated hybrid of kaolinite with KH2po4 showing high ionic conductivity (~10-4 s cm-1) at room temperature. Solid State Sci. 74, 95–100. http://dx.doi.org/10.1016/j.solidstatesciences.2017.10.007.

Mahy, J.G., Lambert, S.D., Léonard, G.L.M., Zubiaur, A., Olu, P.Y., Mahmoud, A., Boschini, F., Heinrichs, B., 2016. Towards a large scale aqueous sol–gel synthesis of doped TiO2: Study of various metallic dopings for the photocatalytic degradation of p-nitrophenol. J. Photochem. Photobiol. A 329, 189–202. http://dx.doi.org/10.1016/j.jphotochem.2016.06.029.

Misra, A.J., Basu, A., Ghosh, A., Habeeb, H.R., Tiwari, N., Mishra, A., Lundborg, C.S., Tripathy, S.K., 2022. Photocatalytic disinfection of multidrug resistant staphylococcus haemolyticus and *Escherichia coli* using visible-LED: A photochemical approach to curb nosocomial infection. Environ. Technol. Innov. 27, http://dx.doi.org/10.1016/j.eti.2022.102502.

Misra, A.J., Das, S., Habeeb Rahman, A.P., Das, B., Jayabalan, R., Behera, S.K., Suar, M., Tamhankar, A.J., Mishra, A., Lundborg, C.S., Tripathy, S.K., 2018. Doped ZnO nanoparticles impregnated on kaolinite (clay): A reusable nanocomposite for photocatalytic disinfection of multidrug resistant *Enterobacter sp.* under visible light. J. Colloid Interface Sci. 530, 610–623. http://dx.doi.org/10.1016/j.jcis.2018.07.020.

Nmiri, A., 2017. Synthesis and characterization of kaolinite-based geopolymer: Alkaline activation effect on calcined kaolinitic. J. Mater. Environ. Sci. 8, 676–690, http://www.jmaterenvironsci.com/.

Nodehi, R., Shayesteh, H., Kelishami, A.R., 2020. Enhanced adsorption of congo red using cationic surfactant functionalized zeolite particles. Microchem. J. 153, http://dx.doi.org/10.1016/j.microc.2019.104281.

Panda, A.K., Mishra, B.G., Mishra, D.K., Singh, R.K., 2010. Effect of sulphuric acid treatment on the physico-chemical characteristics of kaolin clay. Colloids Surf. A Physicochem. Eng. Asp. 363, 98–104. http://dx.doi.org/10.1016/j.colsurfa.2010.04.022.

Panias, D., Giannopoulou, I.P., Perraki, T., 2007. Effect of synthesis parameters on the mechanical properties of fly ash-based geopolymers. Colloids Surf. A Physicochem. Eng. Asp. 301, 246–254. http://dx.doi.org/10.1016/j.colsurfa.2006.12.064.

Paredes-Quevedo, L.C., Castellanos, N.J., Carriazo, J.G., 2021. Influence of porosity and surface area of a modified kaolinite on the adsorption of basic red 46 (BR-46). Water Air Soil Pollut. 232, http://dx.doi.org/10.1007/s11270-021-05450-3.

Ptáček, P., Kubátová, D., Havlica, J., Brandštetr, J., Šoukal, F., Opravil, T., 2010. The non-isothermal kinetic analysis of the thermal decomposition of kaolinite by thermogravimetric analysis. Powder Technol. 204, 222–227. http://dx.doi.org/10.1016/j.powtec.2010.08.004.

Qtaitat, M.A., Al-Trawneh, I.N., 2005. Characterization of kaolinite of the Baten El-Ghoul region/south Jordan by infrared spectroscopy. Spectrochim Acta A Mol. Biomol. Spectrosc. 61, 1519–1523. http://dx.doi.org/10.1016/j.saa.2004.11.008.

Qu, M., Ma, X., He, J., Feng, J., Liu, S., Yao, Y., Hou, L., Liu, X., 2017. Facile selective and diverse fabrication of superhydrophobic, superoleophobic-superhydrophilic and superamphiphobic materials from kaolin. ACS Appl. Mater. Interf. 9, 1011–1020. http://dx.doi.org/10.1021/acsami.6b10964.

Reli, M., Kočí, K., Matějka, V., Kovář, P., Obalová, L., 2014. Effect of calcination temperature and calcination time on the kaolinite/TiO2 composite for photocatalytic reduction of CO2. GeoSci. Eng. 58, 10–22. http://dx.doi.org/10.2478/v10205-011-0022-2.

Saikia, B.J., Parthasarathy, G., 2010. Fourier transform infrared spectroscopic characterization of kaolinite from Assam and Meghalaya, Northeastern India. J. Mod. Phys. 01, 206–210. http://dx.doi.org/10.4236/jmp.2010.14031.

Selvan, B.K., Thiyagarajan, K., Das, S., Jaya, N., Jabasingh, S.A., Saravanan, P., Rajasimman, M., Vasseghian, Y., 2022. Synthesis and characterization of nano zerovalent iron-kaolin clay (nZVI-kaol) composite polyethersulfone (PES) membrane for the efficacious As2O3 removal from potable water samples. Chemosphere 288, http://dx.doi.org/10.1016/j.chemosphere.2021.132405.

Shayesteh, H., Rahbar-Kelishami, A., Norouzbeigi, R., 2015. Adsorption of malachite green and crystal violet cationic dyes from aqueous solution using pumice stone as a low-cost adsorbent: Kinetic, equilibrium, and thermodynamic studies. Desalination Water Treat. 57, 12822–12831. http://dx.doi.org/10.1080/19443994.2015.1054315.

Soleimani, M.A., Naghizadeh, R., Mirhabibi, A.R., Golestanifard, F., 2012. Effect of calcination temperature of the kaolin and molar Na2O/SiO2 Activator ratio on physical and microstructural properties of metakaolin based geopolymers. Iran. J. Mater. Sci. Eng. 9, 43–51.

Tang, W., Zhang, S., Sun, J., Li, H., Liu, X., Gu, X., 2017. Effects of surface acid-activated kaolinite on the fire performance of polypropylene composite. Thermochim. Acta. 648, 1–12. http://dx.doi.org/10.1016/j.tca.2016.12.007.

Tao, Q., Su, L., Frost, R.L., Zhang, D., Chen, M., Shen, W., He, H., 2014. Silylation of mechanically ground kaolinite. Clay Miner. 49, 559–568. http://dx.doi.org/10.1180/claymin.2014.049.4.06.

Tchanang, G., Djangang, C.N., Abi, C.F., Moukouri, D.L.M., Blanchart, P., 2021. Synthesis of reactive silica from kaolinitic clay: Effect of process parameters. Appl. Clay Sci. 207, http://dx.doi.org/10.1016/j.clay.2021.106087.

Thommes, M., Kaneko, K., v. Neimark, A., Olivier, J.P., Rodriguez-Reinoso, F., Rouquerol, J., Sing, K.S.W., 2015. Physisorption of gases, with special reference to the evaluation of surface area and pore size distribution (IUPAC technical report). Pure Appl. Chem. 87, 1051–1069. http://dx.doi.org/10.1515/pac-2014-1117.

Tironi, A., Trezza, M.A., Irassar, E.F., Scian, A.N., 2012. Thermal treatment of kaolin: Effect on the pozzolanic activity. Procedia Mater. Sci. 1, 343–350. http://dx.doi.org/10.1016/j.mspro.2012.06.046.

Torres-Luna, J.A., Carriazo, J.G., 2019. Porous aluminosilicic solids obtained by thermal-acid modification of a commercial kaolinite-type natural clay. Solid State Sci. 88, 29–35. http://dx.doi.org/10.1016/j.solidstatesciences.2018.12.006.

Vicente-Rodriguez, M.A., Suarez, M., Angel Bañares-Muñoz, M., de Dios Lopez-Gonzalez, J., 1996. Comparative FT-IR study of the removal and structural modifications during acid silicates of octahedral cations treatment of several. Spectrochim. Acta Part A 52, 1685–1694.

Yahaya, S., Jikan, S.S., Badarulzaman, N.A., Adamu, A.D., 2017. Effects of acid treatment on the SEM-EDX characteristics of kaolin clay. Path Sci. 3, 4001–4005. http://dx.doi.org/10.22178/pos.26-6.

Yans, J., Lithostratigraphie, 2007. Minéralogie et diagenèse des sédiments à faciès wealdien du bassin de Mons (Belgique). Classe Des Sci., Acad. R. de Belgique IX, 1–179.

Zhao, B., Liu, L., Cheng, H., 2021. Rational design of kaolinite-based photocatalytic materials for environment decontamination. Appl. Clay Sci. 208, http://dx.doi.org/10.1016/j.clay.2021.106098.

Zhou, Y., Cheng, H., Wei, C., Zhang, Y., 2021. Effect of acid activation on structural evolution and surface charge of different derived kaolinites. Appl. Clay Sci. 203, http://dx.doi.org/10.1016/j.clay.2021.105997.

Zhou, C., Liang, Y., Gong, Y., Zhou, Q., Chen, Y., Qiu, X., Wang, H., Luo, W., Yan, C., 2014. Modes of occurrence of Fe in kaolin from Yunnan China. Ceram. Int. 40, 14579–14587. http://dx.doi.org/10.1016/j.ceramint.2014.06.042.

Zhou, C.H., Zhao, L.Z., Wang, A.Q., Chen, T.H., He, H.P., 2016. Current fundamental and applied research into clay minerals in China. Appl. Clay Sci. 119, 3–7. http://dx.doi.org/10.1016/j.clay.2015.07.043.